Refractive Index Sensing Based on Plasmonic Waveguide Side Coupled With Bilaterally Located Double Cavities

Lei Xu, Shun Wang, and Lijun Wu

***Abstract*—Based on a metal–dielectric–metal (MDM) plasmonic waveguide side coupled with a single cavity, we propose a resonator system by placing double cavities on each side of the MDM waveguide. The coupling between two cavities provides an additional degree of freedom to engineer the resonant transmission response. By decomposing the compound cavity modes into two decoupled resonances, we obtain the theoretical transmission response of the resonator system and optimize the geometric parameters to improve the performance of refractive index sensing. At last, we conduct numerical experiments on the theoretically optimized resonator system and find that the resonant wavelength is linearly related with the refractive index of the material filled in the cavities and waveguide. A high sensitivity of 1030 nm/RIU (refractive index unit) is realized in a nanoscale structure (several hundred nanometers). This refractive index sensing configuration is easy to be integrated into lab-on-a-chip and find potential application in plasmonic circuits.**

***Index Terms*—Metal–dielectric–metal (MDM) waveguide, refractive index sensor (RIS), surface plasmon resonance (SPR).**

I. Introduction

REFRACTIVE index sensing has a broad range of applications in many areas such as in life and chemical sciences [1]–[3]. A surface plasmon resonance (SPR) has been widely used in refractive index sensing because the SP field is concentrated at the metal–dielectric interface and the resonant frequency is very sensitive to the refractive index of the nearby dielectric media [4], [5]. An outstanding example of SPR refractive index sensor (RIS) consists of a dielectric prism with a thin layer of metal coating on its top (Kretschmann prism configuration), in which the excitation condition of the SPR is highly sensitive to the refractive index of the metal as well as the dielectric materials near the metal surface. The RIS with this configuration has been commercialized [2], [6]. Although with high sensitivity, this type of RIS is difficult to be integrated into lab-on-a-chip because of the use of the prism and the excitation requirement [7]. Other SPR RISs include those based on the strong extinction (including scattering and absorption) from individual metallic nanoparticles [8] or the extraordinary transmission through nanohole arrays [9], [10]. These RISs are also difficult to be integrated into lab-on-a-chip.

Another typical example of SPR RISs is based on a resonance from a metal–dielectric–metal (MDM) waveguide combined with a Fabry–Perot (FP) cavity [11], [12]. The optical reflection or transmission spectra of this system exhibit a peak or a dip, which has been applied in nonlinear optical switching and RIS, etc. [13]–[18]. Because of a single-mode limit [7], this kind of RIS does not have such high sensitivity as those based on Kretschmann prism configuration. However, its size can be scaled down to be less than 1 μm. Furthermore, its waveguide configuration makes it easy to be integrated into lab-on-a-chip.

As is known, the performance of the SPR-based applications such as sensing [19], [20] and optical switching [13] is largely determined by the width as well as the depth of the dip in the spectral response. In this letter, based on the transmission response of an MDM plasmonic waveguide structure side coupled with a single cavity (SC), we introduce an additional degree of freedom to tune the spectrum response of the resonator system by placing another cavity on the other side of the MDM waveguide. Metal sliver (Ag) is chosen because its SPR can be tuned from visible to near-infrared. By decomposing the complex cavity modes into two decoupled resonances, the transmission response of the system with the MDM waveguide side coupled with bilaterally-located double cavities (BLDCs) can be tailored through modulating the indirect coupling strength between the two cavities via the waveguide. Compared to an MDM plasmonic waveguide structure side coupled with an SC, the resonator system with BLDCs exhibit a sharper shape in the transmission spectrum. In addition, the depth of the dip can be kept near to zero when the loss inside the cavity is considered. These properties can be utilized to improve the performance of the RIS. By adjusting the distance between the cavity and the waveguide, which determines the coupling strength between them, the spectral sensitivity of this novel SPR RIS can reach as high as 1030 nm/RIU in the numerical experiments. This cavity-based RIS with high sensitivity and ultracompact size (several hundred nanometers) can be easily integrated into lab-on-a-chip and find potential application in plasmonic circuits.

II. Analytical Model

We first set up the analytical model to investigate the transmission response of the proposed resonator system. The schematic system is shown in Fig. 1(a), in which the cavity *a* and *b* are side located at the same *y* (as an example) along with the straight

Manuscript received June 12, 2013; revised January 23, 2014; accepted March 6, 2014. Date of publication August 8, 2014; date of current version September 4, 2014. The review of this paper was arranged by Associate Editor M. M. De Souza. This work was supported in part by the Project of High-level Professionals in the Universities of Guangdong Province and the National Natural Science Foundation under Grant 61378082.

The authors are with the Laboratory of Nanophotonic Functional Materials and Devices, School for Information and Optoelectronic Science and Engineering, South China Normal University, Guangzhou 510006, China (e-mail: 555xulei@163.com; ws850720@163.com; 1jwu@scnu.edu.cn).

Color versions of one or more of the figures in this paper are available online at http://ieeexplore.ieee.org.

Digital Object Identifier 10.1109/TNANO.2014.2346392

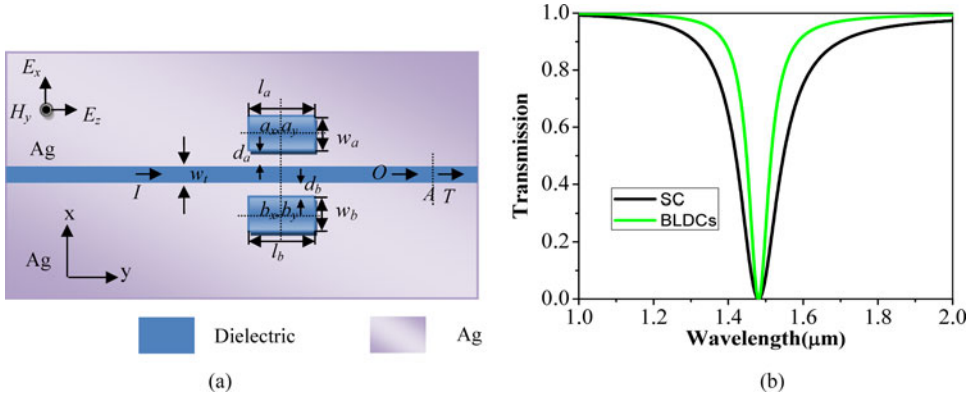

Fig. 1. (a) Schematic of the SPR-based RIS consisting of an MDM plasmonic waveguide coupled with the bilaterally-located double cavities (BLDCs). (b) Theoretical transmission spectra of the resonator system with BLDCs (green line, calculated from (14)) and an SC (black line).

MDM waveguide. When the incident optical wave transmits along the waveguide, part of the wave is coupled into the cavity *a* and *b*, where the forward and backward waves are almost completely reflected at the dielectric–Ag interfaces inside cavities. At the same time, part of the wave is coupled back into the straight MDM waveguide.

Normally, the transmission spectrum of a MDM waveguide side coupled with an SC exhibits a symmetric Lorentzian line shape [21], [22]. At the resonant frequency ω_o, the incident power is reflected and results in a dip $(T_{\min})$ in the transmission spectrum of the structure. The resonant wavelength λ_o is controlled by the geometry of the cavity, i.e., the length L and the width w_o. λ_o can be estimated by combining the resonant condition $(\Delta\phi = m \cdot 2\pi)$ of forming stable standing waves in the cavity and the phase shift $\Delta\phi$ of light passing through the cavity, which is given by

$$\Delta\phi = \frac{4\pi n_{\text{eff}}(\lambda_o) \bullet L}{\lambda_o} \tag{1}$$

where n_{eff} is the effective refractive index of the cavity and is related with λ_o and w_o. Their relationship is determined by [23], [24]

$$\tanh\left(\sqrt{n_{\text{eff}}^2 - \varepsilon_d} \cdot w_o \pi/\lambda_o\right) = \frac{-\varepsilon_d \sqrt{n_{\text{eff}}^2 - \varepsilon_m}}{\varepsilon_m \sqrt{n_{\text{eff}}^2 - \varepsilon_d}}. \tag{2}$$

From (1) and (2), the resonant wavelength λ_o is obviously related with n_{eff}, which is dependent on the refractive index n of the materials filled in the cavities and waveguide. This is the origin of the refractive index sensing in the cavity-based resonator system.

In the BLDCs resonator system as shown in Fig. 1(a), w_a (w_b) and l_a (l_b) are the width and length of cavities; d_a (d_b) denotes the distance between the cavity *a* (*b*) and the waveguide. The eigen-frequency of the cavity ω_a (ω_b) (referring to the resonant frequency of the SC system) is decided by its width w_a (w_b) and length l_a (l_b) [25]. The distance d_a (d_b) controls the coupling strength between the cavity *a* (*b*) and the waveguide. Based on the temporal coupled-mode theory [26], the dynamic equations for the field in the cavity *a* (*b*) can be modeled as

$$\frac{da}{dt} = \left(jw_a - \frac{1}{\tau_a} - \frac{1}{\tau_{0a}}\right)a + j\sqrt{\frac{1}{\tau_a}}I - \frac{1}{\tau_b}b \tag{3}$$

$$\frac{db}{dt} = \left(jw_b - \frac{1}{\tau_b} - \frac{1}{\tau_{0b}}\right)b + j\sqrt{\frac{1}{\tau_b}}I - \frac{1}{\tau_a}a \tag{4}$$

$$O = I + j\sqrt{\frac{1}{\tau_a}}a + j\sqrt{\frac{1}{\tau_b}}b \tag{5}$$

where *I* stands for the incident field into the waveguide and *O* for the output. $1/\tau_a(1/\tau_b)$ is the decay rate due to the field coupling from the cavity into the waveguide which is controlled by the distance between the cavity and the waveguide d_a (d_b). $1/\tau_{0a}$ $(1/\tau_{0b})$ denotes the field decay rate induced by the intrinsic loss of the cavity. In such system, the fields in both cavities will couple with each other only through an indirect pathway (mediated by the waveguide).

When the two cavities are identical, i.e., $l_a = l_b = l_0$ and $w_a = w_b = w_0$, their eigen-frequencies and decay rates are the same: $\omega_a = \omega_b = \omega_0, 1/\tau_{0a} = 1/\tau_{0b} = 1/\tau_0$. The dynamic equations for the field in the cavity *a* (*b*) become

$$\frac{da}{dt} = \left(j\omega_0 - \frac{1}{\tau_a} - \frac{1}{\tau_0}\right)a + j\sqrt{\frac{1}{\tau_a}}I - \frac{1}{\tau_b}b \tag{6}$$

$$\frac{db}{dt} = \left(j\omega_0 - \frac{1}{\tau_b} - \frac{1}{\tau_0}\right)b + j\sqrt{\frac{1}{\tau_b}}I - \frac{1}{\tau_a}a \tag{7}$$

$$O = I + j\sqrt{\frac{1}{\tau_a}}a + j\sqrt{\frac{1}{\tau_b}}b. \tag{8}$$

In this case, the compound cavity modes in the system can be decomposed into two decoupled resonances:

$$\frac{d\mathrm{A}}{dt} = \left(j\omega_0 - \frac{1}{\tau_a} - \frac{1}{\tau_b} - \frac{1}{\tau_0}\right)\mathrm{A} + \left(\frac{1}{\tau_b} - \frac{1}{\tau_a}\right) \times \frac{\frac{\sqrt{2}}{2}j\left(\sqrt{\frac{1}{\tau_a}} - \sqrt{\frac{1}{\tau_b}}\right)}{j\omega - j\omega_0 + 1/\tau_0}I + \frac{\sqrt{2}}{2}j\left(\sqrt{\frac{1}{\tau_a}} + \sqrt{\frac{1}{\tau_b}}\right)I \tag{9}$$

$$\frac{d\mathrm{B}}{dt} = \left(j\omega_0 - \frac{1}{\tau_0}\right)B + \frac{\sqrt{2}}{2}j\left(\sqrt{\frac{1}{\tau_a}} - \sqrt{\frac{1}{\tau_b}}\right)I \tag{10}$$

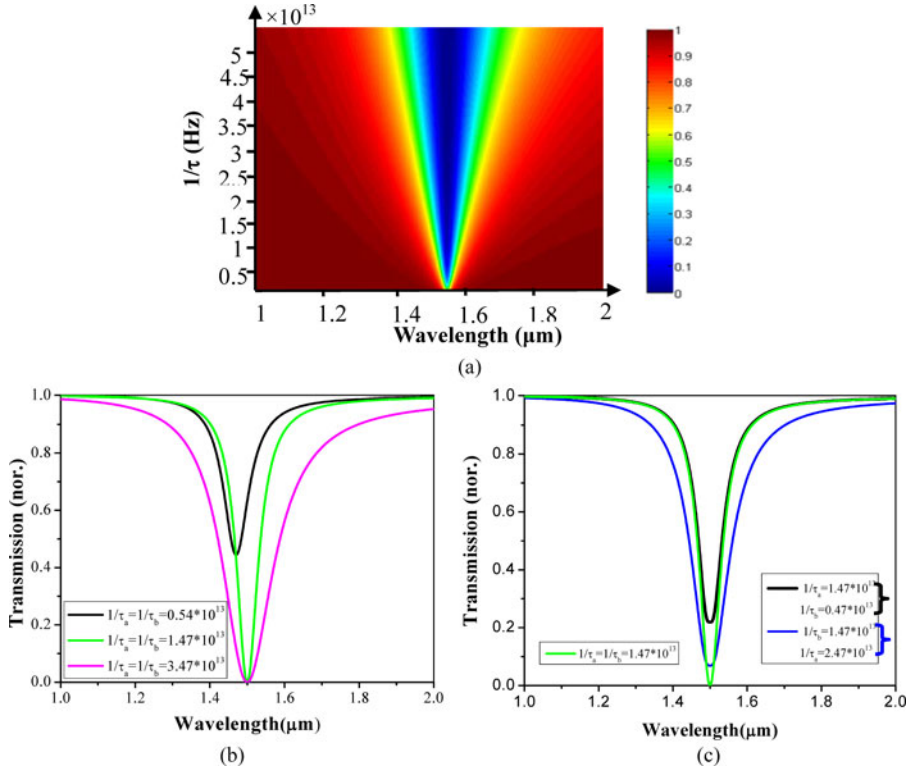

Fig. 2. (a) Evolution for the transmission spectra of the resonator system calculated from (12) as a function of wavelength and decay rate when $1/\tau_a = 1/\tau_b = 1/\tau$. (b) Three typical transmission spectra picked from (a). (c) Transmission spectra by fixing $1/\tau_a$ and tuning $1/\tau_b$ ($1/\tau_a = 1/\tau_b = 1.47 \times 10^{13}$ Hz is demonstrated here for reference). $1/\tau_a$ and $1/\tau_b$ are assumed to be nondispersive here. $1/\tau_0$ is set to be 0.6×10^{13} Hz.

$$O = I + \frac{\sqrt{2}}{2} j \left(\sqrt{\frac{1}{\tau_a}} + \sqrt{\frac{1}{\tau_b}} \right) A + \frac{\sqrt{2}}{2} j \left(\sqrt{\frac{1}{\tau_a}} - \sqrt{\frac{1}{\tau_b}} \right) B \tag{11}$$

where $A = (a+b)/\sqrt{2}, B = (a-b)/\sqrt{2}$. The transmission ($T$) response of the system can then be calculated as

$$T = \left| \frac{O}{I} \right|^2 = \left| 1 - \frac{\left(\sqrt{\frac{1}{\tau_a}} - \sqrt{\frac{1}{\tau_b}} \right)^2}{j(\omega - \omega_0) + \frac{1}{\tau_0}} - \frac{\frac{1}{2}\left(\sqrt{\frac{1}{\tau_a}} + \sqrt{\frac{1}{\tau_b}} \right)^2}{j(\omega - \omega_0) + \frac{1}{\tau_a} + \frac{1}{\tau_b} + \frac{1}{\tau_0}} + \frac{\frac{1}{2}\left(\frac{1}{\tau_b^2} - \frac{1}{\tau_a^2} \right)}{\left[j(\omega - \omega_0) + \frac{1}{\tau_0} \right] \bullet \left[j(\omega - \omega_0) + \frac{1}{\tau_a} + \frac{1}{\tau_b} + \frac{1}{\tau_0} \right]} \right|^2 \tag{12}$$

where $\omega = 2\pi c/\lambda$ is the frequency and ω_o the frequency at resonance. If the distance between the cavity a (b) and waveguide is the same, i.e., $1/\tau_a = 1/\tau_b = 1/\tau$, the transmission response of the system can be simplified as

$$T = \left| \frac{O}{I} \right|^2 = \left| 1 - \frac{\frac{2}{\tau}}{j(\omega - \omega_0) + \frac{2}{\tau} + \frac{1}{\tau_0}} \right|^2 = \frac{(\omega - \omega_0)^2 + \left(\frac{1}{\tau_0} \right)^2}{(\omega - \omega_0)^2 + \left(\frac{2}{\tau} + \frac{1}{\tau_0} \right)^2}. \tag{13}$$

In order to understand the working mechanism, we ignore the loss at first, i.e., $1/\tau_{0a} = 1/\tau_{0b} = 1/\tau_0 = 0$. Then

$$T = \frac{(\omega - \omega_0)^2}{(\omega - \omega_0)^2 + 4\left(\frac{1}{\tau} \right)^2}. \tag{14}$$

The calculated result from (14) is shown in Fig. 1(b) with $1/\tau = 1.47 \times 10^{13}$ Hz. The transmission response of the SC system is also plotted for comparison. Obviously, the transmission spectrum for the BLDCs system exhibits a sharper band edge. To more thoroughly understand the geometric configuration dependence of the transmission response, we conduct theoretical studies on how the decay rate $1/\tau_a (1/\tau_b)$, which is related with the distance between the waveguide and the cavities, influence the transmission spectrum. The calculation is based on (12) in which the loss is considered and $1/\tau_0$ is set to be 0.6×10^{13} Hz, as we have analyzed in our previous paper [27]. The results are shown in Fig. 2(a). As observed, with a decrease of $1/\tau$, the bandwidth of the transmission dip is narrowed down. However, when $1/\tau$ is too small, the dip of the transmission is very shallow, suggesting that the coupling between the cavity and the waveguide is too small. Fig. 2(b) shows three typical transmission spectra for different coupling strength. As seen, the resonant wavelength of the system is blue shifted with the decrease of the coupling strength when the dip shifts away from zero. Fig. 2(c) demonstrates the calculated results when we fix $1/\tau_a$ and tune $1/\tau_b$. As expected, with an increase of $1/\tau_b$, the bandwidth of the transmission dip is also broadened. It is worth noting that the bandwidth is similar in

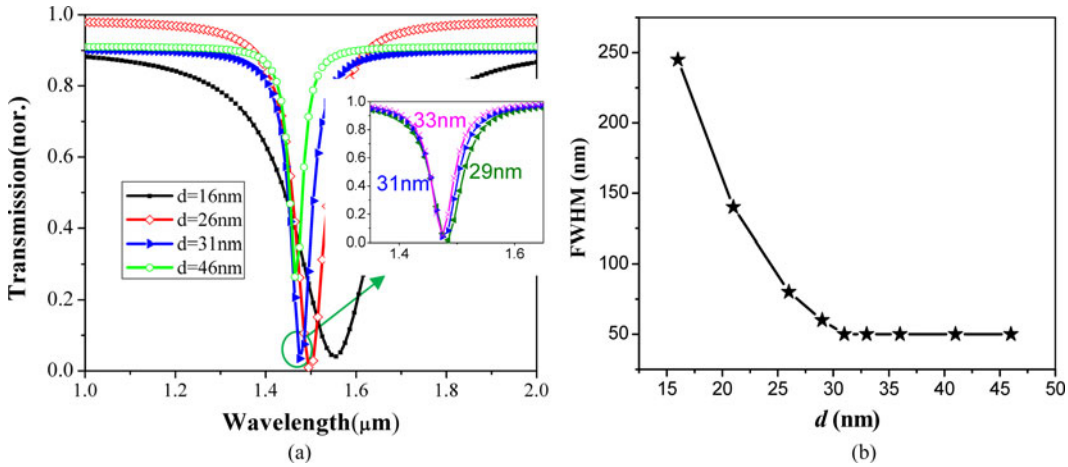

Fig. 3. (a) Transmission response of the resonator system with different distance between the cavity and the straight waveguide by numerical experiments. Inset shows a fine variation of the distance. Compare to the theoretical results illustrated in Fig. 2, the distance $d_a = d_b = 33$ nm roughly corresponds to a decay rate $1/\tau = 1.4710^{13}$ Hz. (b) The relationship between FWHM of the transmission spectrum and the distance between the cavity and the waveguide.

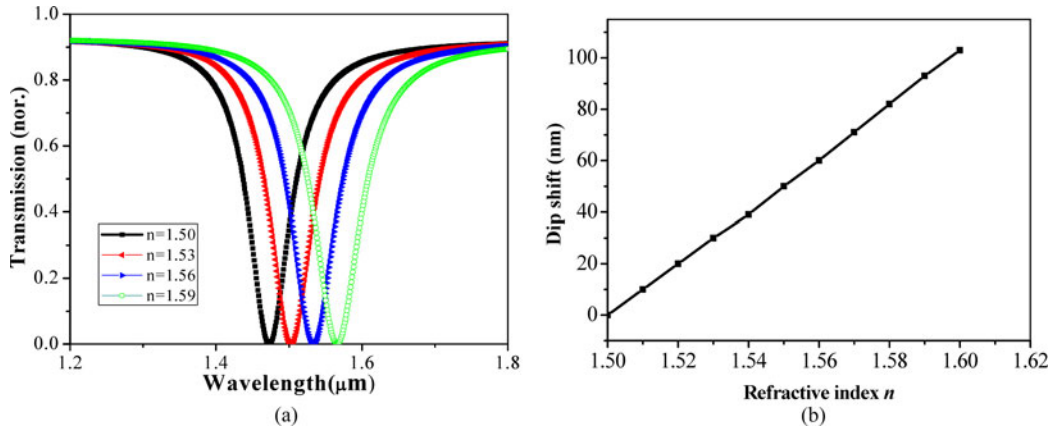

Fig. 4. (a) Numerical transmission spectra of the RIS with different materials filled in the BLDCs and the straight waveguide. The distance is chosen to be $d_a = d_b = 33$ nm. (b) Shift of the wavelength at the resonant dip in the transmission spectrum versus the variation of the refractive index.

the case of $1/\tau_a = 1.47 \times 10^{13}$ Hz, $1/\tau_b = 0.47 \times 10^{13}$ Hz and $1/\tau_a = 1/\tau_b = 1/\tau = 1.47 \times 10^{13}$ Hz. This phenomenon can be attributed to the shift of the resonant wavelength with the coupling strength, as we have analyzed in Fig. 2(b). Consequently, to obtain a sharp resonance dip without losing its depth, the optimum coupling strength between the cavities and the waveguide is $1/\tau_a = 1/\tau_b = 1/\tau = 1.47 \times 10^{13}$ Hz.

In fact, there is another parameter influencing the transmission response of the proposed RIS structure besides the coupling strength. If we define the center position of the cavity a and b as (a_x, a_y), (b_x, b_y), then $a_x = w_a/2 + d_a$, $b_x = w_b/2 + d_b$.

They determine the distance, i.e., the coupling strength between the cavity and the straight waveguide. a_y and b_y describe the relative position along the straight waveguide. If $a_y \neq b_y$, there will be a complex phase shift of the fundamental mode propagating in the waveguide between the two cavities. This is similar to the phenomenon studied in [28]. We are not going to discuss the related details in this letter. Furthermore, the two bilaterally-located cavities are set identical here since different cavities will induce different resonant wavelengths and thus broaden resonant dip, which is not desirable in the application of RIS.

III. Simulation Results

In this section, we utilize a two-dimensional (2-D) finite difference time domain (FDTD) method with a perfectly matched layer (PML) boundary condition to simulate the transmission response of the MDM waveguide structure side coupled with BLDCs based on the analytic results shown in Section II. The spatial grid size and temporal step are set as $\Delta x = 2$ nm, $\Delta z = 2$ nm, and $\Delta t = \Delta x/2\,c$, respectively.

The geometric parameters of the cavities are set as: $l_a = l_b = 360$ nm, width $w_a = w_b = 80$ nm. The width w_t of the waveguide is chosen to be 40 nm which only allows the excitation of the fundamental waveguide mode. The frequency-dependent complex relative dielectric constant of Ag used in our simulations is characterized by the Drude model with $(\varepsilon_\infty,\ \omega_p,\ \lambda) = (4.2,\ 1.346 \times 10^{16}\ \text{Hz},\ 9.61710^{13}\ \text{Hz})$, $\varepsilon_m(\omega) = \varepsilon_\infty - \omega_p^2/\omega(\omega + i\gamma)$ [25]. The fundamental TM mode

of the plasmonic waveguide is incident from the left-hand side of the waveguide. The transmission of the proposed resonator system is normalized to that of a straight MDM waveguide with the same length and thus it does not include the propagation loss of the waveguide.

Fig. 3 plots the transmission response of the resonator system side coupled with BLDCs with different distance between the cavity and the waveguide. The analyte materials filled inside the cavities and waveguide can be gaseous or liquids. Gaseous can be diffused into the cavity based on gas diffusion force in vacuum circumstance and liquids can be filled into the cavity using nanofilling technique based on capillarity attraction [29]–[31]. The refractive index *n* of the analyte materials is set to be 1.5 initially. The distance between the cavity and the waveguide $d_a = d_b$ is set to be 21, 26, 31, 36, and 41 nm, respectively. As observed, with a decrease of the distance (corresponding to an increase of 1/ τ), the coupling between the cavity and the waveguide becomes stronger. Simultaneously, the two decoupled resonances can interfere with each other which leads to a broader bandwidth and sharper lineshape in the transmission response [26]. When the distance is increased from 36 to 41 nm, the coupling between the cavity and waveguide become weak, resulting in a shallow transmission dip. The inset of Fig. 3(a) shows that the lineshape of the transmission spectrum is similar with $d = 29, 31, 33$ nm, suggesting a large fabrication tolerance for the resonator system. As the overall refractive index sensitivity depends both on the FWHM of the transmission response and the shift of the resonant wavelength [32], we plot the relationship between the FWHM and the distance *d* in Fig. 3(b). It can be seen that when $d \geq 31$ nm, FWHM of the transmission response reaches to the smallest value (50 nm) in this system. In order to obtain strong signal in the sensing application, the distance cannot be too large to keep $T_{\min}$ approaching zero at the resonant wavelength.

Fig. 4(a) demonstrates the evolution of the transmission response with the variation of the refractive index *n* at a distance of $d = 33$ nm. Clearly, the transmission spectrum is red shifted with the increase of *n*. Fig. 4(b) plots the shift of the resonant dip wavelength with the change of *n*, from which we can obtain 1030-nm dip wavelength shift per refractive index unit. This high sensitivity together with deep dip resonance is a very important property for RIS applications.

IV. Conclusion

To summarize, we decompose the compound cavity modes in the MDM plasmonic waveguide structure side coupled with BLDCs into two decoupled resonances based on the temporal couple theory. Then we obtain the theoretical transmission spectrum of the proposed resonator system and optimize the geometric configuration to improve the performance for RIS application. Based on the theoretical results, we conduct numerical experiments and obtain an ultracompact (several hundred nanometers) and high-sensitive (1030 nm/RIU) RIS which can be applied in the future lab-on-a-chip.

References

[1] A. J. Haes and R. P. Van Duyne, "A nanoscale optical biosensor: Sensitivity and selectivity of an approach based on the localized surface plasmon resonance spectroscopy of triangular silver nanoparticles," *J. Am. Chem. Soc.*, vol. 124, pp. 10596–10604, 2002.

[2] C. L. Baird and D. G. Myszka, "Review current and emerging commercial optical biosensors," *J. Mol. Recognit.*, vol. 14, pp. 261–268, 2001.

[3] Y. Fang, "Label-free cell-based assays with optical biosensors in drug discovery," *Assay Drug Dev. Technol.*, vol. 4, pp. 583–595, 2006.

[4] J. H. Zhu, X. G. Huang, and X. MEI, "High-resolution plasmonic refractive-index sensor based on a metal-insulator-metal structure," *Chin. Phys. Lett.*, vol. 28, p. 054205, 2010.

[5] M. M. Miller and A. A. Lazarides, "Sensitivity of metal nanoparticle surface plasmon resonance to the dielectric environment," *J. Phys. Chem. B*, vol. 109, pp. 21556–21565, 2005.

[6] R. L. Rich and D. G. Myszka, "Review survey of the year 2006 commercial optical biosensor literature," *J. Mol. Recognit.*, vol. 20, pp. 300–366, 2007.

[7] Z. F. Yu and S. H. Fan, "Extraordinarily high spectral sensitivity in refractive index sensors using multiple optical modes," *Opt. Exp.*, vol. 19, pp. 10029–10040, 2011.

[8] A. J. Haes, S. L. Zou, G. C. Schatz, and R. P. Van Duyne, "A nanoscale optical biosensor: The long range distance dependence of the localized surface plasmon resonance of noble metal nanoparticles," *J. Phys. Chem. B*, vol. 108, pp. 109–116, 2004.

[9] K. A. Tetz, L. Pang, and Y. Fainman, "High-resolution surface plasmon resonance sensor based on linewidth-optimized nanohole array transmittance," *Opt. Lett.*, vol. 31, pp. 1528–1530, 2006.

[10] A. G. Brolo, R. Gordon, B. Leathem, and K. L. Kavanagh, "Surface plasmon sensor based on the enhanced light transmission through arrays of nanoholes in gold films," *Langmuir*, vol. 20, pp. 4813–4815, 2004.

[11] A. Artar, A. A. Yanik, and H. Altug, "Fabry-Pérot nanocavities in multilayered plasmonic crystals for enhanced biosensing," *Appl. Phys. Lett.*, vol. 95, p. 051105, 2009.

[12] T. H. Zhang, S. Talla, Z. C. Gong, S. Karandikar, R. Giorno, and L. Que, "Biochemical sensing with a polymer-based micromachined Fabry-Perot sensor," *Opt. Exp.*, vol. 18, pp. 18394–18400, 2010.

[13] Z. J. Zhong, Y. Xu, S. Lan, Q. F. Dai, and L. J. Wu, "Sharp and asymmetric transmission response in metal-dielectric-metal plasmonic waveguides containing Kerr nonlinear media," *Opt. Exp.*, vol. 18, pp. 79–86, 2009.

[14] B. Brian, B. Sepúlveda, Y. Alaverdyan, L. M. Lechuga, and M. Käll, "Sensitivity enhancement of nanoplasmonic sensors in low refractive index substrates," *Opt. Exp.*, vol. 3, pp. 2015–2023, 2009.

[15] P. Prabhathan, V. M. Murukeshan, Z. Jing, and P. V. Ramana, "Compact SOI nanowire refractive index sensor using phase shifted Bragg grating," *Opt. Exp.*, vol. 17, pp. 15330–15341, 2009.

[16] Q. Liu and K. S. Chiang, "Refractive-index sensor based on long-range surface plasmon mode excitation with long-period waveguide grating," *Opt. Exp.*, vol. 17, pp. 7933–7842, 2009.

[17] X.-S. Lin and X.-G. Huang, "Tooth-shaped plasmonic waveguide filters with nanometeric sizes," *Opt. Lett.*, vol. 33, pp. 2874–2876, 2008.

[18] J.-H. Zhu, X.-G. Huang, J. Tao, X.-P. Jin, and X. Mei, "Nanometeric plasmonic refractive index sensor," *Opt. Commun.*, vol. 285, pp. 3242–3245, 2012.

[19] J. Homola, "On the sensitivity of surface plasmon resonance sensors with spectral interrogation," *Sens. Actuators B*, vol. 41, pp. 207–211, 1997.

[20] A. G. Brolo, R. Gordon, B. Leathem, and K. L. Kavanagh, "Surface plasmon sensor based on the enhanced light transmission through arrays of nanoholes in gold films," *Langmuir*, vol. 20, pp. 4813–4815, 2004.

[21] Z. F. Yu, G. Veronis, and S. H. Fan, "Gain-induced switching in metal-dielectric-metal plasmonic waveguides," *Appl. Phys. Lett.*, vol. 92, p. 041117, 2008.

[22] A. Noual, A. Akjouj, Y. Pennec, J. N. Gillet, and B. Djafari-Rouhani, "Modeling of two-dimensional nanoscale Y-bent plasmonic waveguides with cavities for demultiplexing of the telecommunication," *New J. Phys.*, vol. 11, p. 103020, 2009.

[23] B. Wang and G. P. Wang, "Plasmon Bragg reflectors and nanocavities on flat metallic surfaces," *Appl. Phys. Lett.*, vol. 87, p. 013107, 2005.

[24] Z. H. Han, E. Forsberg, Member, and S. L. He, Senior, "Surface plasmon Bragg gratings formed in metal-insulator-metal waveguides," *IEEE Photon. Technol. Lett.*, vol. 19, pp. 91–93, Jan. 2007.

[25] Q. Zhang, X. G. Huang, X. S. Lin, J. Tao, and X. P. Jin, "A subwavelength coupler-type MIM optical filter," *Opt. Exp.*, vol. 17, pp. 7549–7555, 2009.

[26] C. Manolatou, M. J. Khan, S. Fan, P. R. Villeneuve, and H. A. Haus, "Coupling of modes analysis of resonant channel add-drop filters," *IEEE J. Quantum Electron.*, vol. 35, pp. 1322–1331, Sep. 1999.

[27] X. S. Lin, J. H. Yan, Y. B. Zheng, L. J. Wu, and S. Lan, "Bistable switching in the lossy side-coupled plasmonic waveguide-cavity structures," *Opt. Exp.*, vol. 19, pp. 9594–9599, 2011.
[28] S. Wang, Y. Xu, S. Lan, and L. J. Wu, "Flat-top reflection characteristics in metal-dielectric-metal plasmonic waveguide structure side coupled with cascaded double cavities," *Plasmonics*, vol. 6, pp. 689–695, 2011.
[29] A. Y. Vorobyev and C. Guo, "Metal pumps liquid uphill," *Appl. Phys. Lett.*, vol. 94, pp. 224102–1–224102-3, 2009.
[30] D. Ugarte, T. Stockli, J. M. Bonard, A. Chatelain, and W. A. De Heer, "Filling carbon nanotubes," *Appl. Phys. A: Mater. Sci. Process*, vol. 67, pp. 101–105, 1998.
[31] D. Ugarte, A. Chatelain, and W. A. De Heer, "Nanocapillarity and chemistry in carbon nanotubes," *Science*, vol. 274, pp. 1897–1899, 1996.
[32] L. J. Sherry, S. H. Chang, G. C. Schatz, and R. P. Van Duyne, "Localized surface plasmon resonance spectroscopy of single silver nanocubes," *Nano Lett.*, vol. 5, pp. 2034–2038, 2005.